

Surface Structure of 4-Mercaptopyridine on Au(111): A New Dense Phase

Santiago Herrera, Federico Tasca,[†] Federico J. Williams,[‡] and Ernesto J. Calvo^{*‡}

Departamento de Química Inorgánica, Analítica y Química Física, INQUIMAE-CONICET, Facultad Ciencias Exactas y Naturales, Universidad de Buenos Aires, Ciudad Universitaria, Pabellón 2, Buenos Aires C1428EHA, Argentina

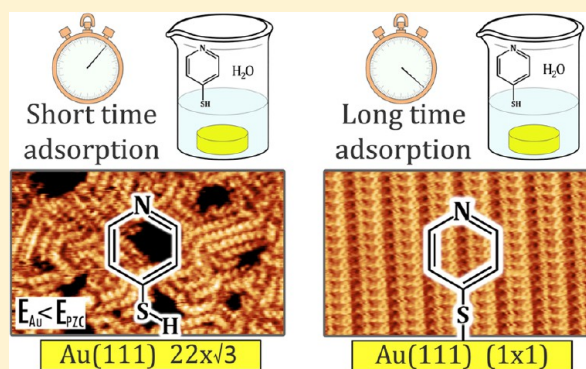
Pilar Carro

Área de Química Física, Departamento de Química, Facultad de Ciencias, Universidad de La Laguna, Instituto de Materiales y Nanotecnología, Avenida Francisco Sánchez, s/n 38200-La Laguna, Tenerife, Spain

Roberto C. Salvarezza

INIFTA Instituto de Investigaciones Fisicoquímicas Teóricas y Aplicadas (INIFTA), Facultad de Ciencias Exactas, Universidad Nacional de La Plata - CONICET- Sucursal 4 Casilla de Correo 16, 1900) La Plata, Argentina

ABSTRACT: 4-Mercaptopyridine (4MPy) self-assembled on Au(111) has been studied by in situ electrochemical scanning tunneling microscopy (EC-STM) in HClO₄, cyclic voltammetry, X-ray photoelectron spectroscopy (XPS) and density functional theory (DFT). Samples prepared by varying the immersion time at constant concentration named short time (30 s) and long time (3 min) adsorption have been studied. Cyclic voltammetry and XPS showed that the chemistry of the adsorbed molecules does not depend on the adsorption time resulting in a well established chemisorbed thiol self-assembled monolayer on Au(111). EC-STM study of the short time adsorption sample revealed a new self-assembled structure after a cathodic desorption/readsorption sweep, which remains stable only if the potential is kept negative to the Au(111) zero charge potential (E_{PZC}). DFT calculations have shown a correlation between the observed structure and a dense weakly adsorbed phase with a surface coverage of $\theta = 0.4$ and a $(5 \times \sqrt{3})$ lattice configuration. At potentials positive to the E_{PZC} , the weakly adsorbed state becomes unstable, and a different structure is formed due to the chemisorption driven by the electrostatic interaction. Long time adsorption experiments, on the other hand, have shown the typical $(5 \times \sqrt{3})$ structure with $\theta = 0.2$ surface coverage (chemisorbed phase) and are stable over the whole potential range. The difference observed in long time and short time immersion can be explained by the optimization of molecular interactions during the self-assembly process.



INTRODUCTION

Self-assembled monolayers (SAMs) of thiols on Au(111) have been extensively studied due to their multiple applications in nanotechnology and also as model systems to understand molecular adsorption on metal substrates.¹ At present it is accepted that thiols (RSH) first physisorb on the Au surface without S–H bond scission and later chemisorb forming a strong RS–Au bond, known as thiolates, and hydrogen with simultaneous lifting of the $(22 \times \sqrt{3})$ surface reconstruction.² Today we have a good understanding of the chemisorption process for aliphatic thiols with a surface coverage $\theta = 0.33$ accompanied by the formation of gold vacancy island and RS–Au_{ad}–RS (Au_{ad} = Au adatom) moieties that are the basic units of the alkanethiol SAMs.³ On the other hand, for small aromatic and heterocyclic thiols, this process results in $\theta =$

0.20/0.25 with the formation of gold islands.⁴ In this case, it is not clear if RS–Au_{ad}–RS or simply RS–Au adsorbates are formed. In particular, scanning tunneling microscopy (STM) has provided a detailed description of the different phases formed along the adsorption time that involve the initial formation of lying down phases (aliphatic)⁵ or highly tilted phases (aromatic)⁶ followed by molecular organization in denser standing up configurations.⁵ By contrast, little is known about the physisorbed state of these molecules on the Au(111) substrate for which we lack structural data.

Received: May 16, 2017

Revised: August 26, 2017

Published: August 29, 2017

In situ STM under electrochemical control is an excellent technique to study the effect of the applied potential of adsorbed molecules on metals. This technique allows one to detect potential induced phase transitions in adsorbed thiols as the surface charge of the substrate is changed. One of the most studied aromatic thiols on Au(111) by in situ STM has been 4-mercaptopyridine (4MPy) in acid media. This interesting thiol, which exposes an N heteroatom to the outer SAM interface, allows one to perform different chemical reactions on the SAM to build complex tridimensional architectures. It is well known that 4MPy decomposes in neutral and alkaline solutions, yielding atomic S on the Au surface, a process that takes minutes to hours to complete but is stable in acid solutions.⁷

Therefore, STM data in acid media have shown that 4MPy organizes in striped rectangular surface structures, namely, a $(5 \times \sqrt{3})$ lattice,^{8–10} with a related $(10 \times \sqrt{3})$ superstructure,¹¹ and a $(7 \times \sqrt{3})$ lattice.¹² DFT calculations without van der Waals interactions have shown that the $(7 \times \sqrt{3})$ is more stable than the $(5 \times \sqrt{3})$.¹³ Interestingly, a more dense $(1 \times \sqrt{3})$ periodicity has been also reported.^{11,12}

In this work we have performed short time adsorption experiments ($t < 1$ min) to form a 4MPy adlayer on Au(111) from aqueous solutions. This adlayer has been placed in the STM-electrochemical cell containing 0.1 M HClO₄ to follow potential induced transformations. EC-STM results reveal the presence of a dense phase when the potential applied (E) to the molecule-Au interface is more negative than the zero charge potential (E_{PZC}). We propose that this dense phase is weakly adsorbed on the Au surface, stabilized by intermolecular π – π interactions and electrostatics forces with the negatively charged substrate, and evolves into a new closely related lattice at $E \geq E_{PZC}$. This intermediate lattice can be transformed into the well-known $(5 \times \sqrt{3})$. When the adsorption time is increased to $t > 2$ min, only the $(5 \times \sqrt{3})$ lattice of chemisorbed 4MPy molecules is observed, irrespective of the applied potential, i.e., the weakly adsorbed state is not observed. Our results demonstrate the existence of dense and organized weakly adsorbed phases of thiols on Au(111), allowing for a complete description and connections between the different surface structures in terms of thermodynamic stability.

EXPERIMENTAL SECTION

4-Mercaptopyridine (95%, Aldrich) and HClO₄ solution (ACS reagent, 60%, Aldrich) were used without further purification. A scanning probe microscope AFM-STM 5500 (AgilentTechnologies) with four-electrode bipotentiostat for the independent control of substrate and tip potentials with respect to the reference electrode in the electrolyte was used for in situ electrochemical scanning tunneling microscopy (EC-STM) measurements. The gold single-crystal electrode used was a solid cylinder (MaTeck, Germany, 1 cm diameter, polished down to 0.03 μm) with one of its ends oriented to better than 1° along the (111) plane. Prior to each experiment, the Au crystal was annealed for 5 min in a hydrogen flame and allowed to cool in air. Tungsten tips were made by electrochemical etching in 2 M KOH and then cleaned with concentrated hydrofluoric acid, water, and acetone. To minimize Faradaic currents, the tips were isolated with nail paint and dried overnight. The custom-made three-electrode PTFE cell was used with two Pt wires used as counter and pseudoreference electrodes, respectively (all potentials herein are referred to Ag/AgCl reference electrode). An HClO₄ 0.1 M aqueous solution was used as supporting electrolyte.

The thiol adsorption was performed by immersion of a clean Au(111) substrate in a freshly prepared 0.27 mM 4MPy aqueous solution (3 mg in 100 mL of Milli-Q water) between 30 s and 3 min depending on the experiment.

Electrochemical desorption measurements were carried out with an Autolab V 30 system (Eco Chemie, Utrecht, The Netherlands) controlled by NOVA 2 Software. A custom-made three-electrode Teflon cell exposing an area of 0.196 cm² was used to hold the gold single crystal. The reference electrode used was AgCl/Ag. For the current density calculation, the electroactive area of the electrode was obtained by integrating the gold reduction peak in the cyclic voltammetry in 0.1 M HClO₄.

X-ray photoelectron spectroscopy (XPS) measurements were conducted in an ultrahigh vacuum (UHV) chamber with a base pressure below 5×10^{-10} mbar, using a 150 mm hemispherical SPECS electron energy analyzer and a monochromatic Al $K\alpha$ X-ray source. Binding energies reported in this work are referenced to the Fermi edge of Au(111) at $E_b = 0$ eV. Atomic ratios were calculated from the integrated intensities of core levels after instrumental and photoionization cross section corrections.

Density functional calculations were performed with the periodic plane-wave basis set code VASP 5.2.12.^{14,15} We have followed the scheme of nonlocal functional proposed by Dion et al.,¹⁶ vdW-DF, and the optimized Becke88 exchange functional optB88-vdW¹⁷ to take into account van der Waals (vdW) interactions. The electronic wave functions were expanded in a plane-wave basis set with a 420 eV cutoff energy. The projector augmented plane wave (PAW) method has been used to represent the atomic cores with PBE potential.¹⁸ Optimal grid of Monkhorst–Pack¹⁹ k-points of $2 \times 9 \times 1$ has been used for numerical integration in the reciprocal space of the $(5 \times \sqrt{3})$ surface structure and we have only considered the Γ point for the $(22 \times \sqrt{3})$ surface structure. Both neutral tautomers 4-mercaptopyridine (4MPy_{HS}) and 1H-pyridine-4-thione (4MPy_{NH}) and 4MPy(S*) radical species were optimized in an asymmetric box of $14 \text{ \AA} \times 16 \text{ \AA} \times 18 \text{ \AA}$. The projector augmented wave (PAW) method,^{18,20} as implemented by Kresse and Joubert,²¹ was employed to describe the effect of the inner cores of the atoms on the valence electrons. The energy minimization (electronic density relaxation) for a given nuclear configuration was carried out using a Davidson block iteration scheme. The dipole correction was applied to minimize polarization effects caused by asymmetry of the slabs.

The surface was modeled by a periodic slab composed of five metal layers for the $(5 \times \sqrt{3})$ surface structure and only three layers for the $(22 \times \sqrt{3})$ due to the large size of the unit cell. In both unit cells, the vacuum layer was of $\sim 14 \text{ \AA}$. Adsorption occurs only on one side of the slab. During the geometry optimization the two bottom layers $(5 \times \sqrt{3})$ and only one $(22 \times \sqrt{3})$ were kept fixed at their optimized bulk truncated geometry for the Au(111) surface. The three $(5 \times \sqrt{3})$ or two $(22 \times \sqrt{3})$ outermost atomic metal layers, as well as the atomic coordinates of the adsorbed species, were allowed to relax without further constraints. The atomic positions were relaxed until the force on the unconstrained atoms was less than 0.03 eV/Å and the tolerance used to define the self-consistency was 10–5 eV for the single point energy. The lattice parameter calculated for bulk Au was 4.16 Å, which compares reasonably well with the experimental value (4.078 Å).

We define the average binding energy (E_b) per 4MPy species adsorbed as follows

$$E_b = \frac{1}{N_{@}} [E_{\text{total}} - E_{\text{Au}(111)} - E_{@}] \quad (1)$$

where $N_{@}$ is the number of adsorbed species in the surface unit cell, E_{total} stands for the total energy of the system, $E_{\text{Au}(111)}$ is the energy of the clean surface, and $E_{@}$ is the energy of the adsorbate either neutral or radical. Negative numbers indicate an exothermic adsorption process with respect to the clean surface and the adsorbed phase originated during the adsorption process.

The Gibbs free energy of adsorption of the surface structure (γ) was approximated through the total energy from DFT calculations by using eq 2:

$$\gamma = \frac{N_{@} E_b}{A} \quad (2)$$

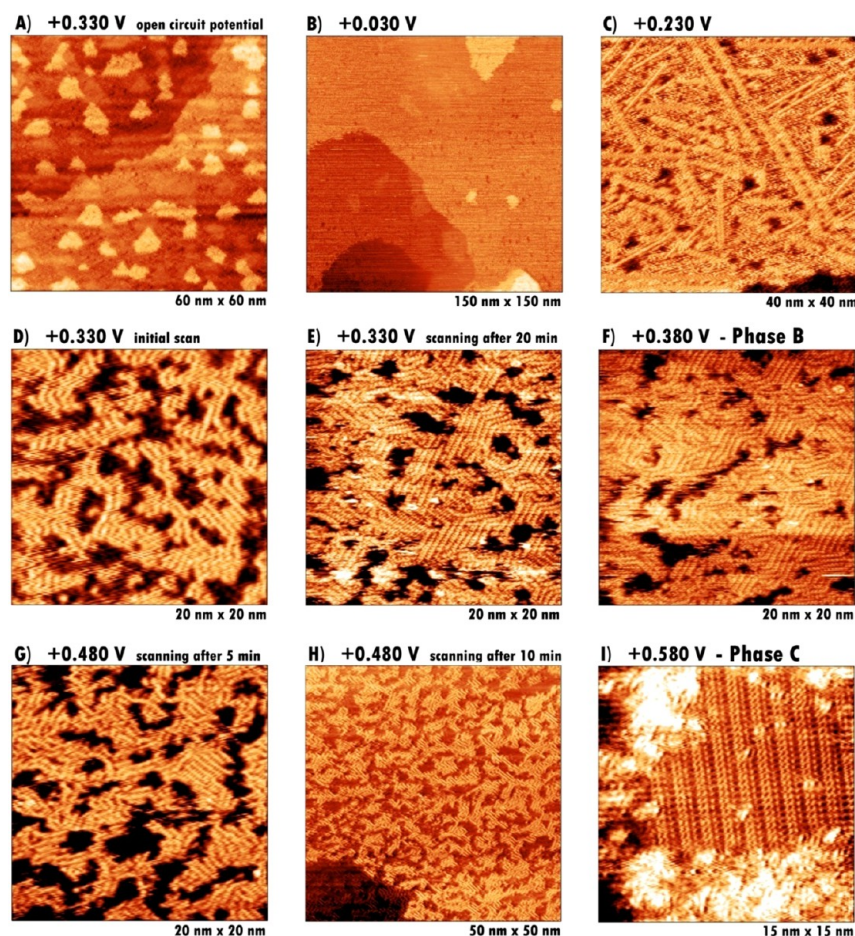


Figure 1. EC-STM images of 30 s adsorption of aqueous 4MPy on Au(111). Sample bias and set point current were fixed to +400 mV and 600 pA, respectively. HClO₄ 0.1 M was used as electrolyte. The substrate potential was sequentially changed to (A) +0.330 V; (B) +0.03 V; (C) +0.230 V; (D) +0.330 V. (E) STM image after scanning for 20 min starting from item D (+0.330 V); (F) +0.380 V (Phase B); (G) STM image after scanning for 5 min at +0.480 V; (H) STM image after scanning for 10 min starting from item G (+0.480 V); (I) +0.580 V (Phase C).

where A is the unit cell area. Considering that we are concerned with free energy differences, it is reasonable to assume that the contributions coming from the configurational entropy, the vibrations, and the work term, pV , can be neglected.^{22,23}

RESULTS AND DISCUSSION

Figure 1 shows typical in situ STM images in 0.1 M HClO₄ of 4-MPy modified Au(111) surface by adsorption at short time. Figure 1A was taken at open circuit potential (ocp), while panels B to I depict the surface morphology at different consecutive applied potentials. The ocp recorded at the beginning of the experiment was $E_{\text{ocp}} = 0.33$ V, a value close to the potential of zero charge of Au(111), $E_{\text{PZC}} = 0.36$ V.²⁴ In Figure 1A, the image reveals Au terraces covered by disordered arrays of molecules and randomly distributed islands over the surface. The cross section analysis shows that the apparent height of these features is 0.24 nm, which corresponds to Au islands that could result from the lifting of the $(22 \times \sqrt{3})$ surface reconstruction induced by the 4MPy adsorption from the 4MPy containing aqueous solution.

When the potential was shifted to $E = 0.03$ V, the Au islands disappeared, suggesting that the $22 \times \sqrt{3}$ surface reconstruction is now the stable surface structure in this potential region (Figure 1B). At this point, a stationary current density has been recorded ($-0.5 \mu\text{A}\cdot\text{cm}^{-2}$), indicating the onset of the hydrogen evolution. If the surface potential is then moved to $E = 0.23$ V,

no islands could be observed, and some ordered domains began to emerge from the completely disordered molecular background structure (Figure 1C). The ordering process is even more evident returning to $E = 0.33$ V, where the molecules now form dense stripes arrays (Figure 1D) whose density increases either with time (Figure 1E) or by increasing the applied potential up to $E = 0.38$ V (Figure 1F). Note, however, that an important fraction of the substrate is not covered by the ordered arrays of molecules (dark regions in Figure 1F). The short-range order surface structure obtained at this point will be named herein as phase B.

Increasing E to 0.48 V, a potential value where the $(22 \times \sqrt{3})$ to (1×1) surface phase transition starts (0.49 V),²⁴ dramatic changes in the molecular structure take place. First, the density of ordered stripes decreases (Figure 1G,H), and finally a new striped structure that we will call phase C with long-range order is clearly visible at $E = 0.58$ V, in coexistence with disordered islands (Figure 1I).

A more detailed analysis of the B phase, which is observed in the 0.3–0.4 V potential region where the $(22 \times \sqrt{3})$ is stable, is shown in Figure 2A,B.

First, the molecular domains of this phase are relatively small (<10 nm) with a short-range order as previously mentioned. The self-assembled molecular stripes intersect themselves forming 60° or 120° angles consistent with the underlying substrate directions (Figure 2A). A closer examination of the

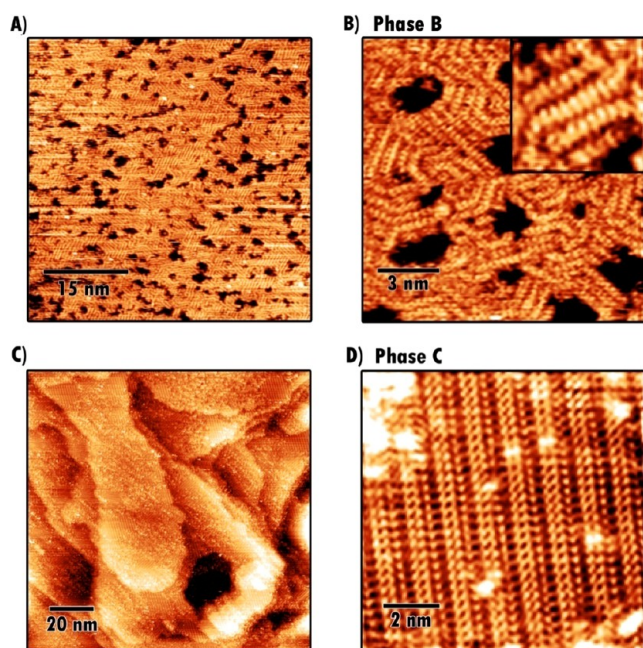


Figure 2. EC-STM images showing a 4MPy/Au(111) self-assembled monolayer (30 s adsorption). (A) Phase B, $E_{\text{sub}} = +330$ V, 50 nm \times 50 nm scan; (B) Phase B, $E_{\text{sub}} = +330$ V, 13 nm \times 13 nm scan (3.75 nm \times 3.75 nm STM high resolution inset); (C) Phase C, $E_{\text{sub}} = +580$ V, 130 nm \times 130 nm scan; (D) Phase C, $E_{\text{sub}} = +580$ V, 10 nm \times 10 nm scan. $E_{\text{bias}} = +400$ mV, $I_{\text{tunn}} = 600$ pA. HClO_4 0.1 M was used as electrolyte.

phase B structure shows that the stripes are separated by 0.53 ± 0.03 nm (Figure 2B) while the distance between molecules is 0.32 ± 0.01 nm (inset in Figure 2B), leading to a surface coverage of $\theta = 0.40$. These structures resembles those observed by in situ STM imaging of bipyridine molecules on the Au(111) surface by Tao et al.²⁵ The large density of irregular holes (dark regions in Figure 2) exhibits 0.18 nm in depth, indicating that they are uncovered substrate regions and not vacancy gold pits since 0.24 nm would be expected in that case.

On the other hand, the C phase is observed at 0.58 V (Figure 2C–D), a potential value where the stable structure of the single crystal should be the Au(111)-(1 \times 1). The STM image reveals long-range molecular domains with sizes of about 10 nm. Typical distances between stripes and molecules were found to be 1.32 ± 0.02 nm and 0.33 ± 0.02 nm, respectively. Interestingly, the C phase has the same intermolecular distance as the B phase but much larger interstripe separation.

If a new experiment is carried out, but in this case the adsorption time is increased up to 2.5–3 min, the phase A is obtained after a few scans at open circuit potential ($E_{\text{ocp}} = +0.390$ V). Note that in this case as in the previous one, the concentration of the 4MPy aqueous solution was carefully fixed to be 0.270 mM. Figure 3 shows that phase A exhibits long-range molecular domains with sizes of about 10–20 nm. Each domain consists of stripes that also intersect themselves following the underlying substrate directions as in the phase B.

Some disordered regions between the ordered domains are also observed by STM. A few holes 0.24 nm in depth (dark regions in the images) corresponding to vacancy gold islands are also observed in the figure. The analysis of the characteristic distances of the surface structure shows 1.44 ± 0.01 nm stripe separation (Figure 3B) and 0.53 ± 0.02 nm intermolecular

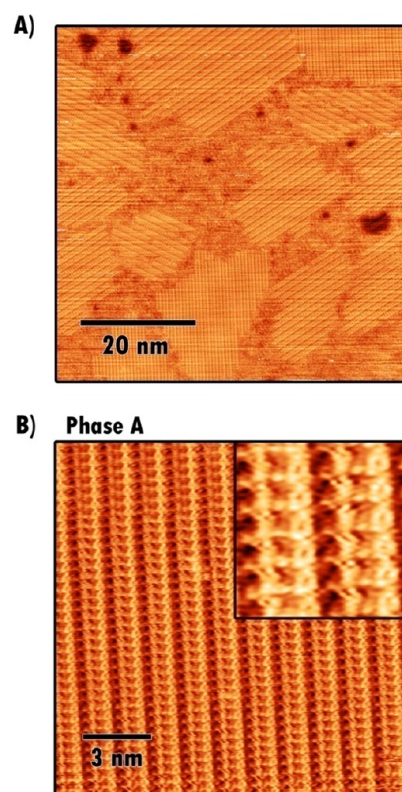


Figure 3. EC-STM images showing a 4MPy/Au(111) phase A self-assembled monolayer (2.5 min adsorption). $E_{\text{sub}} = +0.390$ V, $E_{\text{tip}} = +0.03$ V, $I_{\text{tunn}} = 600$ pA. (A) 60 nm \times 60 nm scan; (B) 15 nm \times 15 nm scan (3.1 nm \times 3.1 nm STM high resolution inset). HClO_4 0.1 M was used as electrolyte.

distance inside the stripes. These figures correspond to the well-known ($5 \times \sqrt{3}$) lattice with $\theta = 0.20$ already reported by several authors in acid media.^{26,27} Interestingly, this phase is now stable irrespective of the applied potential. In fact, this phase was imaged in the whole potential range before reaching a potential of $E = +0.03$ V where complete disorder of the 4MPy molecules was observed resulting in an apparent clean Au surface (hydrogen evolution region). Figure 4A to 4D show consecutive STM imaging of phase A starting from ocp, going down to +0.03 V and then going up to +0.580 V (intermediate images between +0.130 V and +0.580 V show the same feature seen in Figure 4D).

In order to estimate the amount of 4MPy resulting from the self-assembly process, reductive desorption measurements were performed in alkaline solution after 4MPy adsorption for either 30 s or 3 min (Figure 5). In both cases, a charge density of $q = 35 \pm 5 \mu\text{C cm}^{-2}$ was obtained, a figure that for one electron transfer results in $\theta = 0.15$, closer to that expected for the diluted ($5 \times \sqrt{3}$) lattice. The presence of a hump at -0.78 V can be assigned to 4MPy molecules adsorbed at step edges.

Figure 6 shows the C 1s, S 2p, N 1s, and O 1s XPS spectra corresponding to the 30 s and 2.5 min respectively 4MPy modified Au(111) surface. The C 1s spectra show a broad signal centered at 284.9 eV corresponding to the different carbon environments in the molecule. The S 2p spectra show the expected doublet corresponding to the S 2p_{3/2} (162.1 eV) and S 2p_{1/2} (163.3 eV) with a 2:1 intensity ratio. The binding energy position of the sulfur peak and the absence of other contribution in this spectral region indicate that all the

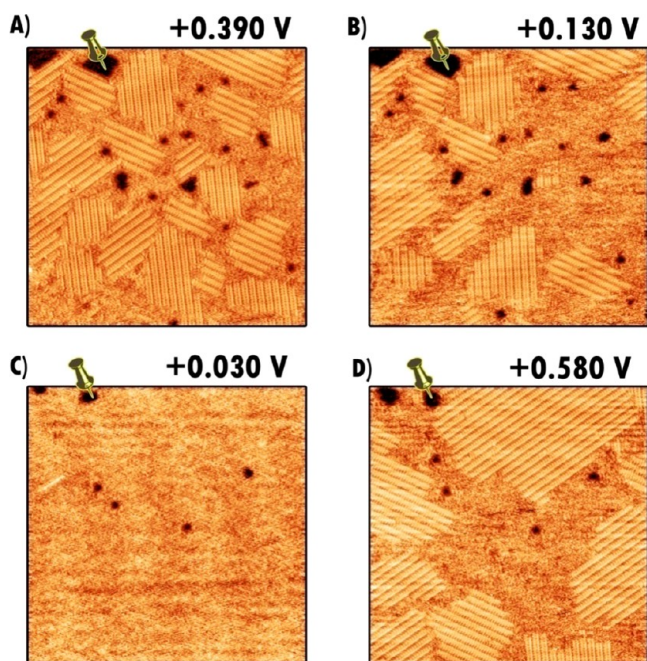


Figure 4. Thiol desorption and stability of phase A over a wide potential window. (A) Initial scan at $E = 0.390$ V (ocp); (B) scan at $E = 0.130$ V (after A); (C) thiol desorption at $E = 0.03$ V; (D) phase A thiol readsorption at $E = 0.130$ V, same feature observed from $E = 0.130$ V to $E = 0.580$ V. $E_{\text{bias}} = +400$ mV, $I_{\text{tunn}} = 600$ pA. Scan size 40×40 nm. HClO_4 0.1 M was used as electrolyte.

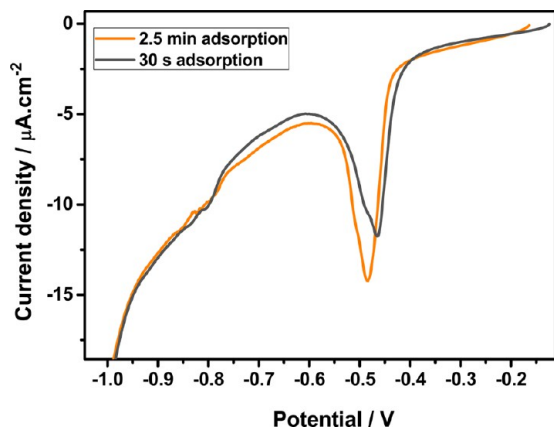


Figure 5. Reductive desorption of a 4MPy/Au(111) self-assembled monolayer (at 30 and 2.5 s adsorption) in KOH 0.1 M. Scan rate: $20 \text{ mV}\cdot\text{s}^{-1}$.

molecules are chemisorbed via a Au–S bond²⁸ after 30 s and 2.5 min of exposure to the aqueous 4MPy solution. The S/Au ratio signal is similar in both samples with an estimate surface coverage 0.15, in good agreement with the electrochemical measurements. Here we should note that these are ex situ measurements of the previously modified surface under no electrochemical potential control. This implies that the dense phase from the STM observations requires an electrochemical bias in order to form.

The N 1s region shows three contributions. The lowest binding energy signal centered at 398.5 eV is due to the deprotonated N atoms in the pyridine molecule, whereas the 400.2 and 401.8 eV contributions are due to N atoms in different degrees of H acceptance and protonation in the

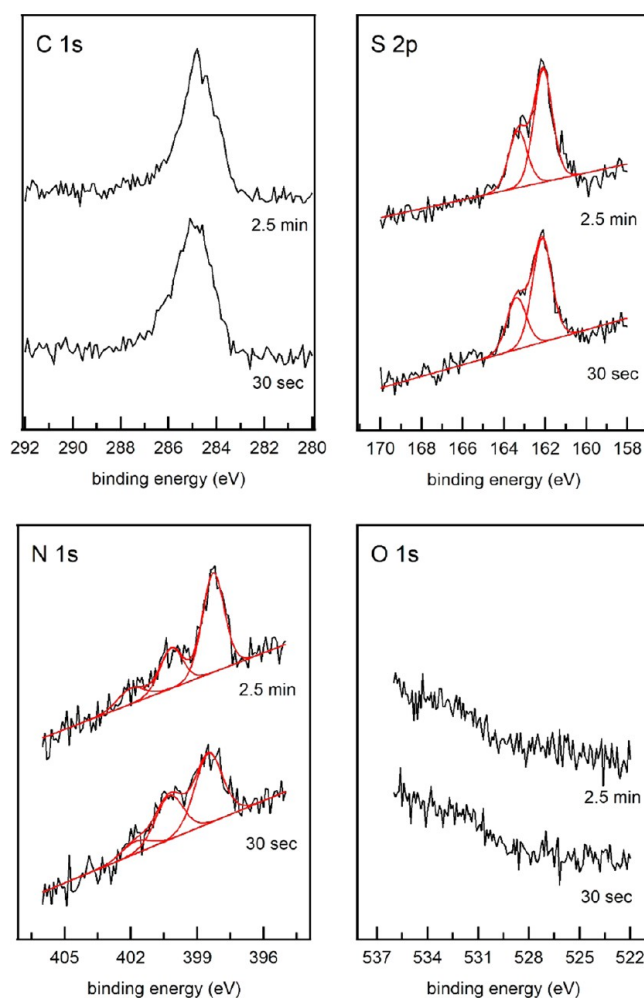


Figure 6. C 1s, S 2p, N 1s, and O 1s XPS spectra after exposing the Au(111) surface to an aqueous solution of 4-mercaptopyridine for 30 s and 2.5 min.

pyridine molecules.^{29,30} The different intensities of each contribution differ in both cases due to the different degrees of protonation in both cases (the pH of the rinsing solution was not controlled). The XPS calculated C:N:S ratios are 5.2:1:0.96 and 5.1:1:1 for 30 s and 2.5 min, respectively. The excellent agreement with the 5:1:1 stoichiometric ratio implies that the molecules retain their molecular identity upon adsorption. Finally the O 1s spectra show a very small contribution at approximately 532.5 eV, presumably due to water molecules attached to the pyridine molecules via H bonds.

Therefore, the XPS and electrochemical data indicates that that no significant differences exist in the chemistry and the surface coverage of the molecular adlayer in the 30 s to 3 min time range used for the self-assembly process. Also, the absence of a peak at -0.9 V and the 161 eV component in the S 2p spectra, as well as the STM images where neither the typical $(\sqrt{3} \times \sqrt{3})R30^\circ$ and rectangular sulfur structures can be observed, are clear evidence that no significant amounts of sulfur contamination is present on the Au(111) surface.³¹

Now we will discuss the connection between diluted A and dense B phases. While the A phase has been unambiguously assigned to the $(5 \times \sqrt{3})$, the surface structure of phase B remains controversial. A dense $(1 \times \sqrt{3})$ phase has been reported for 4MPy at lower E values in H_2SO_4 media, but the authors claim that the dense phase is never observed in HClO_4

media at any potential.¹¹ In that case, a complex adlayer with bisulfate anions coadsorbed on the protonated pyridinium N atoms in order to decrease repulsive interactions has been proposed. By contrast, the dense B phase presented in this work is observed in HClO₄ by playing with the molecule adsorption time. Also, a dense phase with nearest neighbor distances as small as 0.21 nm has been reported for 4MPy in acid media, suggesting that the molecules are adsorbed as disulfide species.⁵² However, the structures observed in these previous works are inconsistent with the 0.32 nm distance measured in our images which coincides with those expected for molecular stabilization by π - π interactions between aromatic heterocycles.

In order to understand the surface structure and chemistry of the dense phase we have made DFT calculations for the well-known ($5 \times \sqrt{3}$) lattice with $\theta = 0.2$ for the 4MPy* (Figure 7a) and compared them with dense ($5 \times \sqrt{3}$) lattice phases of 4MPy* (Figure 7b) and of the thione tautomer (4MPy_{NH}) (Figure 7c) ($\theta = 0.4$), both consistent with the STM

intermolecular distances. Also we have studied the adsorption of the 4MPy_{SH} species on both the Au(1 × 1), ($5 \times \sqrt{3}$), $\theta = 0.40$ (Figure 7d) and ($22 \times \sqrt{3}$), $\theta = 0.41$ (Figure 7e,f) Au surfaces. The optimized structures are shown in Figure 7a–f and their corresponding geometrical and energetic parameters are included in Table 1. First, the 4MPy_{NH} species adsorbs

Table 1. Structural and Energetic Parameters for the 4MPy*, 4MPyH_{NH}, and 4MPy_{SH} Models

surface lattice	$(5 \times \sqrt{3})$				$(22 \times \sqrt{3})$	
	adsorbate	4MPy*	4MPy*	4MPy _{NH}	4MPy _{SH}	
θ		0.2	0.4	0.4	0.4	0.41
E_b /eV		-2.10	-2.04	-0.85	-0.90	-0.81
γ /meV·Å ⁻²		-56.20	-108.92	-45.60	-48.2	-44.10
$Z(S-Au_{\text{surf}})/\text{Å}$		1.93	1.93	2.34	2.82	2.80/3.10
$\alpha(N-S-$ normal _{surface})/°		39.5	40.6	43.1	37.0	36.0
Bader	S	-0.09	-0.11	+1.2	+1.33	+1.32
charge/e	Au	+0.01	+0.05	-0.01	-0.04	0.00

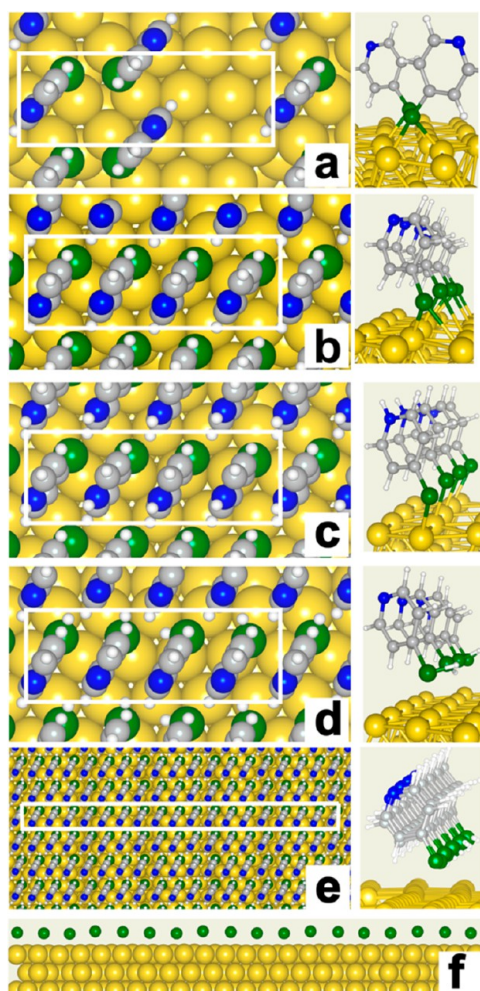


Figure 7. Optimized surface models for 4-mercaptopyridine on Au(111). Right, top view and left side view. (a) ($5 \times \sqrt{3}$) 4MPy* $\theta = 0.2$. (b) ($5 \times \sqrt{3}$) 4MPy* $\theta = 0.4$. (c) ($5 \times \sqrt{3}$) 4MPy_{NH} $\theta = 0.4$. (d) 4MPy_{SH} $\theta = 0.4$, e) 4MPy_{SH} ($22 \times \sqrt{3}$) $\theta = 0.41$. (f) Side view of ($22 \times \sqrt{3}$) surface model where only S atoms of 4MPy_{SH} are shown, the surface corrugation is 0.3 Å. Key: yellow, Au atoms; green, S atoms; gray, C atoms; blue, N atoms; white, H atoms. The unit cells of the surface structures (white) are indicated.

close to the substrate but exhibits a small adsorption energy (E_b) and less stable (less negative) surface free energy (γ) than the diluted and dense 4MPy* species. On the other hand, the 4MPy_{SH} on both Au substrates exhibits similar low E_b and lower γ values than the 4MPy_{NH} species although it exhibits much larger S–Au distances (≈ 3 Å) suggesting a physisorbed state. Interestingly, while the diluted ($5 \times \sqrt{3}$) chemisorbed lattice exhibits much higher E_b than those of the 4MPyH_{NH} and 4MPy_{SH} physisorbed lattices the difference in γ values is much smaller ($\Delta\gamma = 8/10$ meV Å⁻²). The stability of these species at ($E < E_{PZC}$) arises from two contributions: (1) the π - π interactions that results in the development of closely packed molecular chains and uncovered substrate regions, (2) electrostatic interactions between the large positive charge of the S atom and the negatively Au substrate atoms which are revealed by the Bader analysis (Table 1).

While we do not know if the ($22 \times \sqrt{3}$) reconstruction is lifted, the STM images of phase B closely resemble the bipyridine patterns adsorbed on Au(111) that has been assigned to physisorbed molecules on the reconstructed surface.²⁵ However, the DFT calculations result in similar stability for 4MPy_{SH} on the (1 × 1) and ($22 \times \sqrt{3}$) surfaces, i.e., it is not possible to assess the state of the molecule–Au interface.

When the potential reaches $E > E_{PZC}$ (the Au surface becomes positive), the S–H bond of the 4MPyH species should be broken, and the thiol radical is adsorbed on the Au substrate. In this case, the Bader analysis indicates charge transfer that results in a slightly negative charge on the S atom and slightly positive charge on the Au atoms (Table 1). Note that, in this case, the thione tautomer should be expelled from the positively charged Au surface, but it can be immediately readsorbed under the thiol form, yielding adsorbed thiol radical.

On the other hand, the dense ($5 \times \sqrt{3}$) chemisorbed lattice (Figure 7b) exhibits the largest stability (the more negative γ value); therefore, in principle, this phase appears as the best candidate to organize the 4MPy molecules on the Au(111) surface. However, there is a problem with the dense phases: the surface coverage of the self-assembled 4MPy molecules before the in situ STM experiments under electrochemical control always yields smaller values than 0.15. Therefore, we need to explain how the system rearranges the 4MPy molecules in

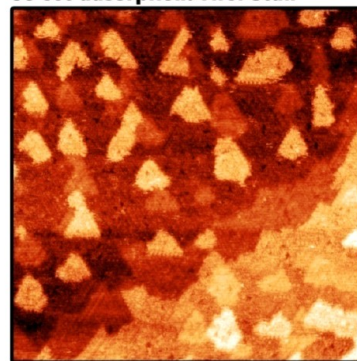
order to have dense and diluted regions distributed on the Au(111) surface in order to have an average surface coverage of 0.15. It is evident that the dense chemisorbed phase, which has not only molecule–molecule but also strong molecule–substrate interactions (large E_b), should be largely impeded to reorganize the molecules. On the other hand, the weakly adsorbed dense phases, which have very weak molecule–substrate interactions (very small E_b), can easily rearrange the initial material into dense patches optimizing molecule–molecule interactions, thus resulting in uncovered regions as shown in the STM images. However, this model also has a weak point: the XPS data show that the initial 4MPy monolayer is chemisorbed. A key piece of evidence about the nature of the dense B phase is that the self-assembled monolayer remains stable only if $E < E_{PZC}$, where the gold surface is negatively charged, i.e., it cannot be detected by XPS. Therefore, we propose that the dense B phase corresponds to weakly adsorbed 4MPy molecules (4MPy_{SH}, 4MPy_{NH}) stabilized by S(+)-Au(-) electrostatic interactions (Table 1). This particular scenario can be obtained by first setting the deposition time to 30 s in the self-assembly step and then performing an electrochemical annealing in which the molecules are first forced to be desorbed (close to the hydrogen evolution region) and then readsorbed over the surface by pushing the potential back again to 0.33 V. Note that atomic H is effective to desorb alkanethiol molecules from the Au(111) surface.³³

When $E > E_{PZC}$, the Au surface becomes positive and the oxidative thiol adsorption takes place, resulting in S–H bond breaking and charge transfer between the Au surface to the S atom, leading to the chemisorbed C phase depicted in Figure 2c,d. This process implies a redistribution of molecules on the Au(111)-(1 × 1) with larger inter row distances, perhaps caused by a decrease in the repulsion of the surface dipoles arising from the charge transfer. We suggest that the C phase, which is incommensurate with the Au(111) surface, is a bridge between the B and A phases since we can move from the C phase to the A phase by simple reordering of the 4MPy molecules. Note, however, that along with this complex process it is also possible that chemisorbed and physisorbed molecules coexist on the substrate surface.

The final question is why the Au samples immersed for 30 s and 2.5 min in the 4MPy containing solution, in spite of showing the same surface chemistry and coverage, differ in their behavior when the cathodic excursion is performed, in the first case leading to the weakly adsorbed B phase and in the second case remaining covered by the phase A. In order to approach the subject, EC-STM images of freshly prepared substrates (first scan-imaging) are taken into consideration.

After a few seconds of reaction, the interaction between the substrate and the 4MPy produces a typical surface covered with a homogeneous distribution of gold islands and no local domains of self-assembly ordering (Figure 8A). If the self-assembly reorganization process is not forced to be stopped at this point, the interaction between the molecules continues, the gold islands begin to disappear, and, after a few minutes, some domains of a stable ($5 \times \sqrt{3}$) structure are formed (Figure 8B). Then we propose that at short immersion time the system is unable to optimize the vdW interactions among the molecules so that they can be easily desorbed during the cathodic excursion relative to those present in the 2.5 min immersed samples. This is not surprising, as it is well-known for alkanethiolates SAMs that, while chemisorption is a fast

A) 30 sec adsorption. First Scan



B) 2.5 min adsorption. First Scan

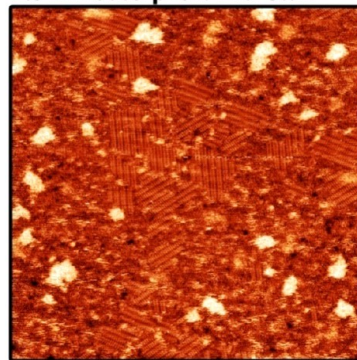


Figure 8. EC-STM images showing 4MPy/Au(111) self-assembled. 60 nm × 60 nm scan, $E_{\text{bias}} = +400$ mV, $I_{\text{tunn}} = 600$ pA, HClO₄ 0.1 M. (A) First scan of 30 s adsorption sample at $E_{\text{OCP}} = +0.330$ V; (B) first scan of 2.5 min adsorption sample at $E_{\text{OCP}} = +0.390$ V.

process, optimization of molecule–molecule interactions is a rather slow process.²⁸

CONCLUSIONS

We have demonstrated the existence of a dense phase for 4MPy SAMs prepared for short adsorption times and subject to a cathodic excursion of potentials values close to the hydrogen evolution reaction. This phase is stable at $E < E_{PZC}$, where the Au surface is negatively charged. We propose that this dense phase is weakly adsorbed on the Au surface stabilized by intermolecular π – π interactions and electrostatic forces between the positively charged S atoms of the 4MPy_{SH} or 4MPy_{NH} species with the negatively charged substrate surface. The weakly adsorbed adlayer evolves into a closely related chemisorbed lattice at $E \geq E_{PZC}$ that can be easily transformed into the well-known ($5 \times \sqrt{3}$). By contrast, when the adsorption time is increased to $t > 2$ min, only the ($5 \times \sqrt{3}$) lattice of chemisorbed 4MPy molecules is observed, irrespective of the applied potential, i.e., the weakly adsorbed state is not observed. The different behavior against a cathodic excursion can be explained considering the optimization of the molecular interactions at longer times that hinders the desorption–reorganization needed to form the weakly adsorbed state since both samples exhibit the same surface chemistry and coverage. Our results allow a complete description and connections between the different surface structures in terms of thermodynamic stability.

AUTHOR INFORMATION

Corresponding Author

*E-mail: calvo@qf.cen.uba.ar.

ORCID

Federico J. Williams: 0000-0002-6194-2734

Ernesto J. Calvo: 0000-0003-0397-2406

Present Address

[†]Departamento de Química de los Materiales, Facultad de Química y Biología, Universidad de Santiago de Chile, Av. Libertador Bernardo O'Higgins 3363, Santiago, Chile

Author Contributions

The manuscript was written through contributions of all authors. All authors have given approval to the final version of the manuscript.

Notes

The authors declare no competing financial interest.

ACKNOWLEDGMENTS

The authors acknowledge financial support from CONICET, ANPCyT and the University of Buenos Aires. F.T. thanks the Teaching Program of Montevideo Group of Universities, AUGM, for a visit grant to the University of Buenos Aires, and Fondecyt 11130167 and "Proyectos Basales". P.C. thankfully acknowledges MINECO (ENE2016-74899-C4-2-R, AEI-FEDER-UE) and the computer resources provided by the Computer Support Service for Research (SAII) at La Laguna University.

ABBREVIATIONS

EC-STM electrochemical scanning tunneling microscopy; 4MPy 4-mercaptopyridine; SAMs self-assembled monolayers; XPS X-ray photoelectron spectroscopy; DFT density functional theory

REFERENCES

- (1) Love, J. C.; Estroff, L. A.; Kriebel, J. K.; Nuzzo, R. G.; Whitesides, G. M. *Chem. Rev.* **2005**, *105*, 1103.
- (2) Vericat, C.; Vela, M. E.; Benitez, G.; Carro, P.; Salvarezza, R. C. *Chem. Soc. Rev.* **2010**, *39*, 1805.
- (3) Häkkinen, H. *Nat. Chem.* **2012**, *4*, 443.
- (4) Jin, Q.; Rodriguez, J. A.; Li, C. Z.; Darici, Y.; Tao, N. J. *Surf. Sci.* **1999**, *425*, 101.
- (5) Poirier, G. E.; Pylant, E. D. *Science* **1996**, *272*, 1145.
- (6) Pensa, E.; Rubert, A. A.; Benitez, G.; Carro, P.; Orive, A. G.; Creus, A. H.; Salvarezza, R. C.; Vericat, C. *J. Phys. Chem. C* **2012**, *116*, 25765.
- (7) Ramírez, E. A.; Cortés, E.; Rubert, A. A.; Carro, P.; Benítez, G.; Vela, M. E.; Salvarezza, R. C. *Langmuir* **2012**, *28*, 6839.
- (8) Cai, W. B.; Wan, L. J.; Noda, H.; Hibino, Y.; Ataka, K.; Osawa, M. *Langmuir* **1998**, *14*, 6992.
- (9) Wan, L. J.; Terashima, M.; Noda, H.; Osawa, M. *J. Phys. Chem. B* **2000**, *104*, 3563.
- (10) Wan, L.-J.; Hara, Y.; Noda, H.; Osawa, M. *J. Phys. Chem. B* **1998**, *102*, 5943.
- (11) Baunach, T.; Ivanova, V.; Scherson, D. A.; Kolb, D. M. *Langmuir* **2004**, *20*, 2797.
- (12) Zhou, W.; Baunach, T.; Ivanova, V.; Kolb, D. M. *Langmuir* **2004**, *20*, 4590.
- (13) Kücera, J.; Gross, A. *Langmuir* **2008**, *24*, 13985.
- (14) Kresse, G.; Hafner, J. *Phys. Rev. B: Condens. Matter Mater. Phys.* **1993**, *48*, 13115.
- (15) Kresse, G.; Furthmüller, J. *Comput. Mater. Sci.* **1996**, *6*, 15.
- (16) Dion, M.; Rydberg, H.; Schröder, E.; Langreth, D. C.; Lundqvist, B. I. *Phys. Rev. Lett.* **2004**, *92*, 246401.
- (17) Klimeš, J.; Bowler, D. R.; Michaelides, A. J. *Phys.: Condens. Matter* **2010**, *22*, 022201.
- (18) Blöchl, P. E. *Phys. Rev. B: Condens. Matter Mater. Phys.* **1994**, *50*, 17953.
- (19) Monkhorst, H. J.; Pack, J. D. *Phys. Rev. B* **1976**, *13*, 5188.
- (20) Blöchl, P. E.; Margl, P.; Schwarz, K. In *Chemical Application of Density-Functional Theory*; Brian, B., Laird, R. B. R., Ziegler, T., Eds.; American Chemical Society: Washington, DC, 1996; Vol. 629, p 54.
- (21) Kresse, G.; Joubert, D. *Phys. Rev. B: Condens. Matter Mater. Phys.* **1999**, *59*, 1758.
- (22) Torres, D.; Carro, P.; Salvarezza, R. C.; Illas, F. *Phys. Rev. Lett.* **2006**, *97*, 226103.
- (23) Reuter, K.; Scheffler, M. *Phys. Rev. B: Condens. Matter Mater. Phys.* **2001**, *65*, 035406.
- (24) Kolb, D. M.; Schneider, J. *Electrochim. Acta* **1986**, *31*, 929.
- (25) Cunha, F.; Tao, N. J. *Phys. Rev. Lett.* **1995**, *75*, 2376.
- (26) Sawaguchi, T.; Mizutani, F.; Taniguchi, I. *Langmuir* **1998**, *14*, 3565.
- (27) Sawaguchi, T.; Mizutani, F.; Yoshimoto, S.; Taniguchi, I. *Electrochim. Acta* **2000**, *45*, 2861.
- (28) Vericat, C.; Vela, M. E.; Corthey, G.; Pensa, E.; Cortés, E.; Fonticelli, M. H.; Ibañez, F.; Benitez, G. E.; Carro, P.; Salvarezza, R. C. *RSC Adv.* **2014**, *4*, 27730.
- (29) Boland, T.; Ratner, B. D. *Langmuir* **1994**, *10*, 3845.
- (30) Ptasíńska, S.; Stypczyńska, A.; Nixon, T.; Mason, N. J.; Klyachko, D. V.; Sanche, L. *J. Chem. Phys.* **2008**, *129*, 065102.
- (31) Lusteinberg, P. G.; Vericat, C.; Benitez, G. A.; Vela, M. E.; Tognalli, N.; Fainstein, A.; Martiarena, M. L.; Salvarezza, R. C. *J. Phys. Chem. C* **2008**, *112*, 11394.
- (32) Wan, L. J.; Noda, H.; Hara, Y.; Osawa, M. *J. Electroanal. Chem.* **2000**, *489*, 68.
- (33) Kautz, N. A.; Kandel, S. A. *J. Am. Chem. Soc.* **2008**, *130*, 6908.